Master in Chemical Engineering

Structured carbon materials for wastewater treatment

A Master's dissertation

by

Ana Isabel Ramos Morgado

Developed within the Dissertation course unit

Performed at Laboratory of Separation and Reaction Engineering - Laboratory of Catalysis and Materials

Associate Laboratory LSRE-LCM

SRE
CM
LABORATÓRIO DE PROCESSOS DE SEPARAÇÃO E REACÇÃO
LABORATÓRIO DE CATÁLISE E MATERIAIS

Supervisors:
Doctor Adrián M.T. Silva
Doctor Cláudia G. Silva
Professor Joaquim L. Faria

U. PORTO
FEUP **FACULDADE DE ENGENHARIA**
UNIVERSIDADE DO PORTO

Department of Chemical Engineering

July, 2017

Acknowledgments

Este trabalho não seria possível sem o apoio e colaboração de algumas pessoas a quem tenho que agradecer.

Em primeiro lugar ao meu orientador Doutor Adrián Silva pelo seu apoio na realização da minha dissertação e pelas oportunidades que me deu.

À minha orientadora Doutora Cláudia Silva tenho a agradecer toda a compreensão e todo o conhecimento científico que partilhou comigo.

Ao Professor Joaquim Faria por me ter dado a oportunidade de investigar nesta área e pela partilha de conhecimentos. Agradeço também a disponibilização do material e espaço do qual é responsável.

Ao Professor Doutor José Luís Figueiredo por ter disponibilizado todos os recursos técnicos do Laboratório de Catálise e de Materiais do qual é diretor.

A todos os meus colegas do laboratório, em especial à Maria José Lima por ter sempre uma palavra amiga, por ter despertado o meu gosto pela investigação e especialmente por estar sempre disposta em me ajudar. À Maria José Sampaio que sempre me apoiou durante estes meses e por ter partilhado comigo muito do seu conhecimento cientifico. Á Raquel, ao João, à Eliana e ao Diogo por me terem recebido tão bem no laboratório e por estarem sempre disponíveis para tudo.

Por último tenho que agradecer à minha mãe e ao meu pai, ao Pedro e ao Bruno por me apoiarem incondicionalmente em todos os momentos, sem eles nada seria possível. À Minda e à Carmen que sempre estiveram presentes em todas as etapas da minha vida.

A toda a minha família e a todos os meus amigos que de uma maneira ou outra sempre estiveram disponiveis para me ouvir e aconselhar. À Juliana, à Débora e à Ana, as minhas amigas de sempre.

Abstract

Photocatalytic processes using semiconductor catalysts have earned increasing importance in the field of wastewaters treatment. Titanium dioxide (TiO_2) is the catalyst of election for this type of application. Nevertheless, mostly due to its low absorption in the visible region of the electromagnetic spectrum, many efforts have been directed towards the development of other photocatalysts with visible light-response.

Graphitic carbon nitride (g-C_3N_4) is a polymeric layered material composed by carbon and nitrogen (with some minor content of hydrogen from terminal condensed amine groups), all earth abundant elements. Its unique electronic and optical properties make it suitable to be used as photocatalyst, in particular if the possibility of being photo-excited with visible light is considered.

Phenol and its derivatives can be found in a wide range of industrial effluents. They are known as toxic and refractory organic compounds and hard to be removed from water using conventional biological treatment processes. In this context, phenol is a well-known molecule used in many studies in this field, so making it one suitable candidate to act as model pollutant.

In the present work, g-C_3N_4 was prepared by thermal decomposition of dicyandiamide. A posterior thermal treatment was performed at 500 ℃ under air. The resulting catalyst was labelled as T500. The efficiency of this and other catalysts was evaluated under Visible-LED irradiation (417 nm) and compared to the commercial TiO_2 material (P25 from Evonik).

During phenol degradation, hydrogen peroxide (H_2O_2) was found to evolve in the presence of T500. To understand the photocatalytic mechanism, assays using phenol aqueous solutions and neat ultrapure water (i.e. without phenol) were performed in the presence of g-C_3N_4 and under vis-LED irradiation. Residual amounts of H_2O_2 were detected in neat ultrapure water, contrasting with the significant concentration of H_2O_2 generated for the experiments using phenol aqueous solutions. The work was followed varying several operating conditions such as catalyst load, initial concentration of phenol and light emission source. Additionally, the effects of pH solution, temperature and the presence of Fe in solution were also studied.

Among the heterogeneous systems tested, the T500 catalyst had the highest efficiency for phenol degradation and production of H_2O_2. The degradation of phenol was improved when iron was added to the initial solution (i.e. photo-Fenton like conditions). Under these conditions, the production of H_2O_2 was also more efficient, the highest concentration produced being registered as 0.598 mmol L^{-1}. The improved degradation of phenol was explained by the production of additional hydroxyl radicals (HO˙) in the photo-Fenton reaction. The formation of by-products from phenol degradation was also investigated. The total organic carbon removal was analysed for selected experiments, from which was concluded that complete mineralization of phenol was not achieved. Finally, triethanolamine and *tert*-butyl alcohol were used in order to better understand the photocatalytic mechanism in the presence of g-C_3N_4.

Resumo

Os processos fotocalíticos baseados no uso de catalisadores semicondutores têm ganho uma importância crescente no que respeita ao tratamento de águas residuais. O dióxido de titânio (TiO_2) é um catalisador de eleição para este tipo de aplicações. No entanto, principalmente devido à baixa absorção ótica na gama do visível do espectro electromagnético, muito do esforço de investigação têm sido direcionado no sentido de desenvolver fotocatalisadores dotados de capacidade de resposta por ativação com luz visível.

O nitreto de carbono grafítico (g-C_3N_4) é um material polimérico constituído por folhas grafíticas de carbono e nitrogénio (com algum hidrogénio proveniente dos grupos amina terminais), todos estes elementos abundantes na superfície terrestre. A conjugação e um conjunto de propriedades eletrónicas e óticas únicas fazem com que este material se adeque a ser usado como fotocatalisador, com a particularidade de poder ser foto-excitado com luz visível.

O fenol e os seus derivados são poluentes comuns a um ampla gama de efluentes industriais. Como compostos de natureza orgânica são conhecidos pela sua toxicidade e difícil remoção do meio aquoso usando processos convencionais de tratamento biológico. Neste contexto, o fenol é uma molécula bem conhecida, muito utilizada como poluente modelo nesta área de investigação.

O g-C_3N_4 usado no presente trabalho, foi preparado por decomposição térmica da dicianodiamida. Após preparação, foi realizado em corrente de ar, um tratamento térmico posterior a 500 °C. O catalisador resultante foi designado por T500. A eficiência deste e de outros catalisadores foi avaliada debaixo de irradiação com LED a emitir na gama do visível (417 nm), sendo depois comparada com o material comercial de referência, o TiO_2 (P25 da Evonik).

Durante a degradação fotocatalítica do fenol, na presença do T500 observou-se a formação de peróxido de hidrogénio (H_2O_2). De forma a perceber o mecanismo fotocatalítico, realizaram-se ensaios com soluções aquosas de fenol e água ultrapura (i.e. sem fenol) na presença de g-C_3N_4 e sob irradiação por LED-vis. Foram detetadas quantidades residuais de H_2O_2 quando as experiências foram levadas a cabo em água ultrapura, ao passo que na presença de fenol se observou a formação de concentrações muito significativas. Foram depois realizadas experiências variando as diversas condições reaccionais, como a quantidade de catalisador, a concentração inicial de fenol e a fonte de emissão de radiação utilizada. Além disso, estudou-se o efeito do pH, da temperatura e da presença de Fe em solução.

De entre os sistemas heterogéneos estudados, o catalisador T500 revelou-se o mais eficiente na degradação de fenol e na produção de H_2O_2. A degradação de fenol foi melhorada quando se adicionou Fe à solução inicial (i.e. condições semelhantes à do processo de foto-Fenton). Nestas condições, a produção de H_2O_2 também foi mais eficiente, atingindo um concentração gerada de 0.598 mmol L^{-1}. A melhor remoção de fenol é explicado pela maior geração de radicais hidroxilo ($HO^•$) pela reação de foto-Fenton. Foi também estudada a formação de

subprodutos de degradação do fenol. Determinou-se a remoção de carbono orgânico total para um conjunto de experiências selecionadas, das quais se concluiu que a mineralização completa do fenol não foi atingida. Por último, foi utilizado a trietanolamina e o *tert*-butanol para tentar compreender melhor o mecanismo fotocatalítico em ação na presença do g-C_3N_4.

Palavras Chave: Fotocatálise; nitreto de carbono grafítico; fenol; peróxido de hidrogénio; foto-Fenton.

Declaration

I hereby declare, on my word of honour, that this work is original and that all non-original contributions were properly referenced with source identification.

Ana Isabel Ramos Morgado

Index

List of Figures

List of Tables

Notation and Glossary

X	Conversion	%

Greek Letters

λ	Wavelength	nm

Roman letters

S_{BET}	Brunauer-Hemmett-Teller Specific Surface Area	$m^2\,g^{-1}$

List of Acronyms

BQ	Benzoquinone
CB	Conduction band
CT	Catechol
e^-	Electron
Eg	Gap energy
Fe^{2+}	Ferrous cation
$g\text{-}C_3N_4$	Graphitic carbon nitride
H^+	Hydrogen ion
h^+	Hole
$HO^{\bullet}$	Hydroxyl radical
HO^-	Hydroxyde ion
HPLC	High performance liquid chromatography
HQ	Hydroquinone
LED	Light emitting diode
P25	Titanium dioxide P25 from Evonik®
NPOC	Non-purgeable organic carbon
O_2^-	Superoxide species
SEM	Scanning electron microscopy
t-BuOH	tert-butyl
TEM	Transmission electron microscopy
TEOA	Triethanolamine

TiO$_2$	Titanium dioxide
TOC	Total organic carbon
UP H$_2$O	Ultrapure water
UV	Ultraviolet
UV-vis	Ultraviolet-visible
VB	Valence band
vis	Visible

1 Introduction

1.1 The role of structured carbons in waste water treatment

Photocatalysis is known as an efficient and relatively low cost and easy operating technology that can be used for water treatment [1]. This work will concentrate on the development of carbon based materials that can use light as activation agent to initiate the cleavage of chemical bonds and hence the destruction of unwanted chemicals. As a bonus to the degradation process, the production of hydrogen peroxide (H_2O_2) will be explored as a mean to potentiate an advanced oxidation process (AOP).

Graphitic carbon nitride (g-C_3N_4) can be synthesized through solvent-free routes starting from low-cost nitrogen and carbon rich compounds. The prepared methods are simple and its surface chemistry, morphology and texture can be modified by simple modification of the preparation process without significant alteration of the overall composition. Since the Sun visible light makes about 43% of the total irradiation spectrum that hits the earth surface, [2] there has been a huge increase on the research to develop visible-light-responsive photocatalysts. With its bandgap of 2.7 eV, g-C_3N_4 expands its absorption into visible region, up to a limit on wave-length absorption of 450 nm, which is an enormous advantage when compared with other semiconductors used in heterogeneous photocatalysis [3]

The specific objectives established for this work were:

- The synthesis and characterization of g-C_3N_4 nitride catalysts.
- The photocatalytic degradation of phenol using g-C_3N_4 catalysts with simultaneous production of H_2O_2.
- The study of the influence of several operating parameters (catalyst load, initial phenol concentration), in the efficiency of phenol degradation.
- To assess the possibility of implementing the photo-Fenton process for the degradation of phenol using the *in-situ* generated H_2O_2.

1.2 Organization of the dissertation

This dissertation is organized in five main chapters. In Chapter 1 the topic of heterogeneous photocatalysis for wastewater treatment using g-C_3N_4 is briefly introduced. Then in Chapter 2, there is presented a literature review on the use of g-C_3N_4 as semiconductor photocatalyst in several instances, mainly focusing on the case of photocatalytic degradation of pollutants. This chapter also addresses the possibility of generating H_2O_2 and the mechanism of this photocatalytic reaction. Another section of this manuscript, Chapter 3, is devoted to the technical concepts under use during the work here described. A technical description of equipment and materials used in this study is undertaken.

The main body of results is compiled in Chapter 4, where the discussion of the reported findings is simultaneously delivered. The synthesis and performances of g-C_3N_4 in the conversion of

phenol are used as pretext to establish the mechanisms of photocatalytic degradation, with the concomitant formation of H_2O_2. The possibility of expanding the treatment to a Fenton-like process, using the *in situ* produced H_2O_2 is also referred. The final Chapter 5 presents the conclusions that could be taken from this study and some suggestions for further project development.

2 State-of-the-art in g-C₃N₄ photocatalysis

2.1 Principles and applications of photocatalysis

Photo-initiated methods are very appealing and promising technologies because they are potentially able to use solar energy (an inexhaustible source of activation energy) in a range of wide environmental remediation applications, carbon dioxide (CO_2) reduction, disinfection and selective organic transformations [4].

Heterogeneous photocatalysis involves light harvesting by a semiconductor material, charge excitation, charge separation and transfer, and, finally, surface electrocatalytic reactions, as described in Figure 1. The surface morphology and structure of the photocatalysts have a big influence in the harvesting process and the charge excitation is strongly associated with the electronic structure [3, 4].
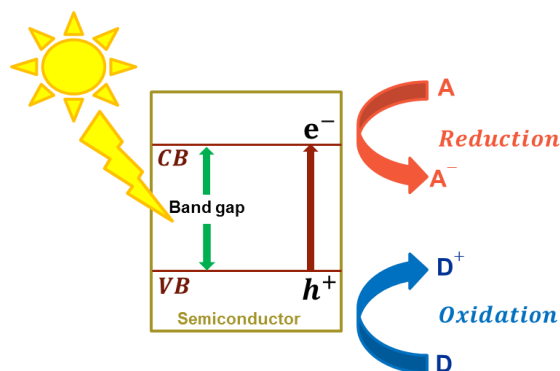
Figure 1 – Schematic representation of the photocatalytic mechanism.

So when reactants come into contact with the light-absorbing semiconductor photocatalyst, the semiconductor material is activated by the photons with energy equal or greater than the band gap energy (Eg). This energy corresponds to the energy between the conduction band and valence band of the material [5]. This photocatalytic reaction starts with the formation of electron-hole pairs followed by an oxidation reaction at the valence band (VB) that acquired a positive charge and a reduction reaction at the conduction band (CB) that attains a negative charge [6].

The thermodynamic driving forces in photocatalytic processes are strongly dependent on the relative relationships between the CB/VB potentials of the semiconductor photocatalysts used and the redox potentials of reversible target reactions. So the more negative CB positions of semiconductors with relation to the redox reactions in water, more prone are the reduction reactions, while the more positive VB positions of semiconductors favor the oxidation reactions [7].

2.2 Semiconductor materials as photocatalysts

Semiconductor photocatalysis possess several advantages compared to classical thermal catalysts, which made them very useful: absence of fouling; lack of mass transfer limitations; applicability at ambient conditions (temperature and pressure); and ability to completely mineralize many organic pollutants into CO_2, water and inorganic ions [6]. Hence the suitable thermodynamic properties, including band gap and CB/VB levels, are alone not responsible for a good photocatalytic efficiency because they can be significantly influenced by many other factors including the structure at micro and nano-levels, adsorption capacity, surface/interface morphology, presence of co-catalysts, crystallinity and, ultimately, the composition of the materials [7].

Titanium dioxide (TiO_2) is the most widely employed photocatalyst owing to its stability, high chemical inertness, relatively low toxicity and low cost. However, the large band gap energy (i.e. the void region covering the top of the filled VB to the bottom of the vacant CB) of TiO_2 (3.2 eV) leads to an absorption edge of 380 nm that restricts the utilization of the broad spectrum of visible solar light. This means that only the ultraviolet (UV) part of the spectrum in the sunlight can be used, accounting for only 4% of the incoming solar irradiation [4].

Besides TiO_2, there are other photocatalysts, like ZnO, which are also capable of being used under UV light. The typical band gap energies of some selected semiconductor photocatalysts are given in Figure 2, with respect to the energy levels of the redox potentials of water reduction oxidation. The CB and VB potentials of the semiconductors are affected by the pH of the solution, but since both are affected in the same way, the band gaps are in general fairly independent of the pH. However, due other surface and structural properties, the majority of those photocatalysts is less efficient compared with TiO_2 in water degradation processes [5].
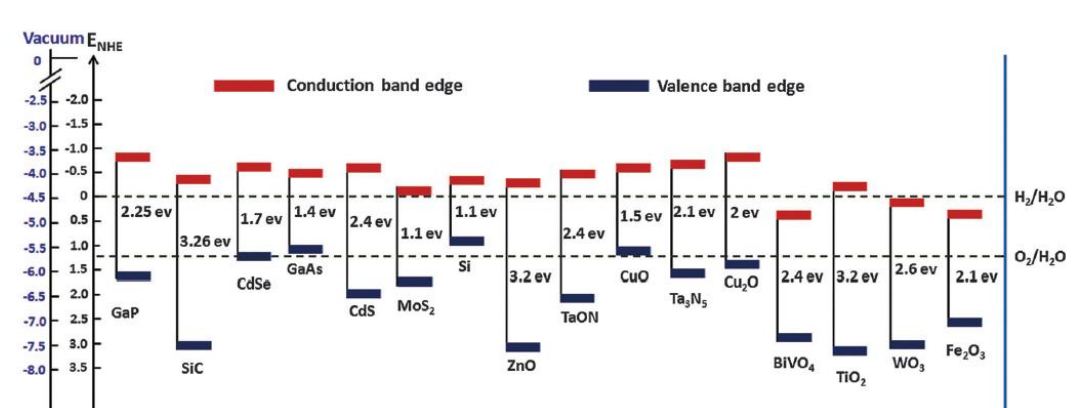
Figure 2 – Schematic representation of the CB and VB position of selected semiconductors used in photocatalysis (adapted from [8]).

2.3 Graphitic carbon nitride as photocatalyst

The conjugated polymer g-C_3N_4 can display very interesting photocatalyst properties as result of its composition and structure: it is a metal-free polymer mainly composed by C and N, with a strong reduction ability, active in visible light, earth-abundant nature, easy fabrication, composed of 2D layered structures, non-toxic and highly stable. Adds to all the fact that g-C_3N_4 also displays the advantages of biocompatibility [4].

Furthermore, g-C_3N_4 could be readily fabricated through normal thermal condensation of several low-cost N-rich organic precursors like urea, thiourea, melamine, dicyandiamide, cyanamide and guanidine hydrochlorid, at temperatures between 500 and 600 °C in air or inert atmosphere [4]. For this work, g-C_3N_4 was prepared using thermal condensation of dicyandiamide.

Another interesting particularity is that pristine g-C_3N_4 and g-C_3N_4 based photocatalysts can be easily assembled with controllable compositions, sizes, thicknesses, pore structures, size distributions and morphologies [4]. The band structures electronic properties, optical absorption and interfacial charge transfer can be readily modeled by different computational packages.

The size of the band gap determines the semiconductor optical properties and color; in fact, g-C_3N_4 displays some florescence properties because electrons can recombine very quickly. If the main role of g-C_3N_4 is to absorb light, produce electron-hole pairs, this formation can also be accompanied by rapid deexcitation pathways, that compete with electron-hole recombination.

The CB of g-C_3N_4 is much more negative than those of conventional inorganic semiconductors, meaning that electrons in g-C_3N_4 possess a large thermodynamic driving force to reduce various kinds of small molecules, like H_2O, CO_2 and O_2 [4].

In Figure 3 it is possible to compare the CB and the VB of g-C_3N_4 with TiO_2. Because the g-C_3N_4 bands are shifted in the direction of the more negative potentials, this suggests that the surface of the g-C_3N_4 does not have the adequate potential to oxidize the hydroxide ion (OH^-) to hydroxyl radical ($HO^{\bullet}$). These radicals are known to be able to degrade most of the organic compounds, which means that, in this case, the mechanism of phenol degradation must be different from those mechanisms derived from typical advanced oxidation processes (AOPs).

The fast recombination of electron-hole pairs is responsible for the reduction of the photocatalysis efficiency (10 ns) in the case of g-C_3N_4 [6]. The substrate g-C_3N_4 has also small surface areas/active sites, high surface inertness, slow reaction kinetics, moderate oxidation ability and low charge carrier mobility.

For this reason, several modification strategies have been pursued to design highly efficient g-C_3N_4-based photocatalysts, including heteroatom doping, layer exfoliation, heterojunction configuration and carbonaceous scaffold [4]. In this work, an exfoliation treatment was used to increase the surface area of g-C_3N_4.
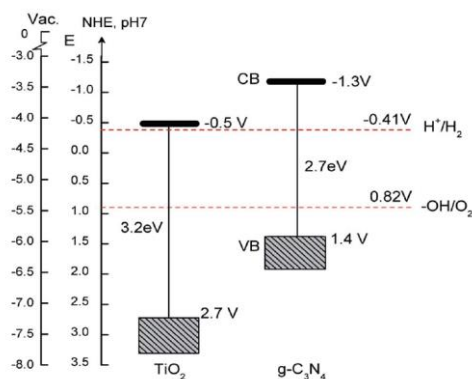
Figure 3 – Band gap for g-C_3N_4 and TiO_2 (adapted from [9]).

2.4 Production of H_2O_2 using g-C_3N_4

Phenol and its derivatives are found in a wide variety of industrial effluents like olive oil mills, petrochemical, pulp and paper industries and are known as toxic and refractory organic compounds, therefore hard to degrade using conventional biological treatment processes [10]. It is important to eliminate these compounds because they are toxic to human beings and they contaminate the environmental compartments (phenol is one of the first compounds included in the list of priority pollutants).

Phenol is often used as model compound in experiments related with water and waste water treatment [10]. In the particular case of photocatalysis, its degradation depends on the light sources (UV, visible and solar), the type of photocatalyst used and respective load, the initial concentration of the pollutant and H_2O_2 (when added), among others. H_2O_2 is a better electron acceptor than oxygen, so the chances for electron/hole recombination decrease [5, 9].

Photocatalytic hydrogen peroxide production from water and molecular oxygen by sunlight is a promising strategy for green, safe and sustainable H_2O_2 synthesis. Hydrogen peroxide is an irreplaceable clean oxidant and is widely used for pulp bleaching and disinfection. It is a potential solar fuel and acts as both oxidant and reductant and can be used for electricity generation [11].

In the heterogeneous photocatalytic process with g-C_3N_4, the reduction reaction (with electrons) is responsible for the formation of hydrogen peroxide and the oxidation reaction (with holes) for the degradation of phenol, Figure 4. The reduction is thus strictly dependent on the oxidation reactions occurring with holes, two electrons being needed in this case, instead of just one like in other photocatalytic mechanisms.
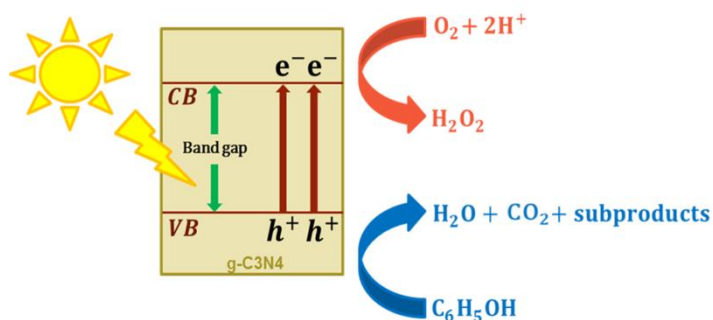
Figure 4 – Heterogeneous photocatalysis using g-C_3N_4.

This mechanism is a particularity for this material due to the $E(O_2/H_2O_2,2e^-)$ of 0.281 V and the C_3N_4 band gap of 2.69 eV [7]. Regardless of the catalyst employed, it is well known that the degradation of phenol typically produces H_2O, CO_2 and some specific by-products like catechol, hydroquinone and benzoquinone, Figure 5. Moreover, oxygen can capture photogenerated electrons and produce reactive radicals by the following reactions.

$$O_2 + e^- \rightarrow O_2^- \qquad (1)$$

$$O_2^- + H^+ \rightarrow HO_2^\bullet \qquad (2)$$

$$HO_2^\bullet + H^+ + e^- \rightarrow H_2O_2 \qquad (3)$$

$$O_2 + 2H^+ + 2e^- \rightarrow H_2O_2 \qquad (4)$$
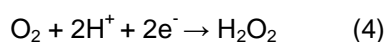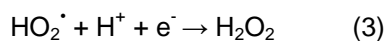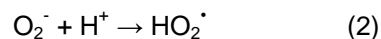
The oxygen reduction on the photocatalyst surface depends on its electronic structure and surface atomic structure [12].
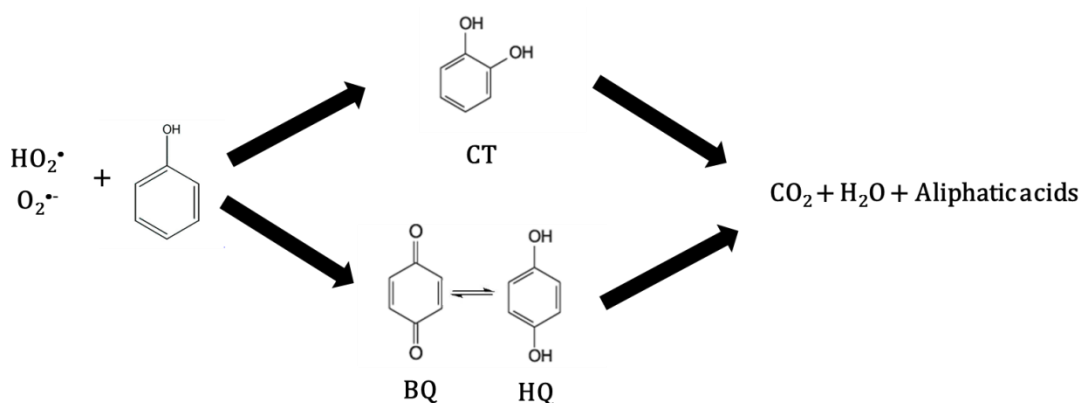
Figure 5 – Heterogeneous photocatalysis (oxidation step) using g-C_3N_4.

2.5 g-C₃N₄ as photocatalyst for water treatment

The application of heterogeneous photocatalysis to prevent environmental contamination is attractive due to its effectiveness in degrading a wide variety of organic water pollutants, like phenol, and also because this process can be sustainable. Nowadays have been studied various advanced oxidative process for degradation of organic dyes in water, including UV/H_2O_2, Fenton/ photo-Fenton schemes, electrochemical catalysis and semiconductor photocatalysis.

The photo-degradation is initiated by branch dissociations (homogeneous reaction). The benzene rings of g-C₃N₄ ideally remain intact and the produced hydroxyl radicals tend to react with the organic molecules over the catalyst surface or in solution [5]. Adding $FeSO_4 \cdot 7H_2O$ as source of Fe species is a way to induce photo-Fenton reactions. The classical Fenton reaction, Equation 5, generates hydroxyl radicals while the irradiation can regenerate Fe^{2+} from Fe^{3+}, Equation 6, 7. In this case the reaction mechanism with g-C₃N₄ is different, Figure 6, since the H_2O_2 spontaneously produced by g-C₃N₄ under irradiation is decomposed (ideally forming hydroxyl radicals) in the presence of iron ions.

$$Fe^{2+} + H_2O_2 \rightarrow Fe^{3+} + OH^\bullet + OH^- \qquad (5)$$

$$Fe^{3+} + H_2O \rightarrow Fe^{2+} + H^+ + HO^\bullet \qquad (6)$$

$$Fe^{3+} + HO^- \rightarrow Fe^{2+} + HO^\bullet \qquad (7)$$
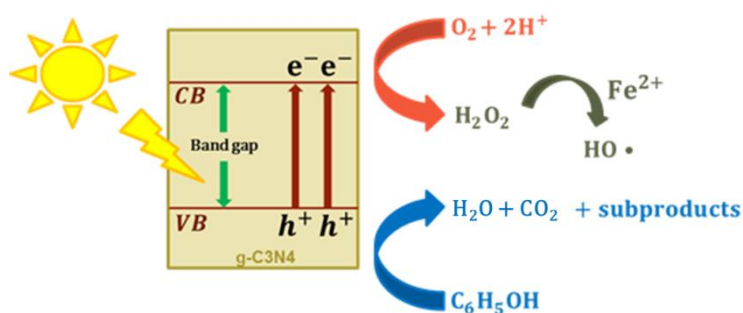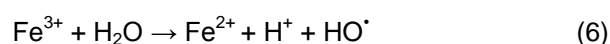
Figure 6 – Heterogeneous photocatalysis using g-C₃N₄ and under photo-Fenton conditions.

Thus, the photo-Fenton process (named after the Fenton's reaction following the 1894 studies of Henry Fenton, on the oxidation reaction of tartaric acid) is an effective way to generate hydroxyl radicals in solution. However, some shortcomings are the narrow pH operating range (near 3) needed to maximize its performance in waste water treatment and the large amounts of iron-reach sludge that is produced [13]. In wastewater treatment there are several concerns when using iron salts as source of Fe^{2+} species such as the generation of sludge wastes when

the pH is increased after the treatment to precipitation the iron species which makes more difficult the follow-up product separation. There are magnetically recoverable catalysts, combination with plants as well as catalyst immobilization in the form of films, or coating, on fixed supports, such as glass slides, raschig rings and beads, stainless steel and polymers that have been used to overcome particles aggregation, formation of slurries and the cost of catalyst separation. [14]

Another alternative is heterogeneous photo-Fenton where are used iron-based solid catalysts that can enable the sunlight harvesting, such as Fe_3O_4 at the same time avoiding the use of excessive amounts of dissolved iron and permitting the easy separation and recovery of the catalysts from the treated waste waters. However, Fe_3O_4 has short carrier diffusion lengths facilitating the electron-hole recombination. [1]

3   Materials and Methods

In this section are described the different experimental techniques, instruments and procedures used in this work.

3.1 Reagents

Dicyandiamide ($C_2H_4N_4$, 99%), titanium (IV) oxysulfate ($TiOSO_4$, 99.99%), phenol (C_6H_5OH, 99%) and clorophenol (C_6H_5ClO, 99%), triethanolamine PA (($HOCH_2CH_2)_3N$, ≥99.5%) sodium hydroxide (NaOH, 97%) and sulfuric acid (H_2SO_4, 95-98%) were obtained from Sigma-Aldrich. Hydrogen peroxide (H_2O_2, 30%) was obtained from Scharlab S.L. Eisen(II)-sulfat heptahydrat ($FeSO_4 \cdot 7H_2O$, 99.5%) and nitrophenol ($C_6H_5NO_3$, 98%) were purchased from Merck. Sodium sulfite anhydrous (Na_2SO_3, ≥98%), metoxyphenol ($H_3OC_6H_4OH$, 99%) and t-butanol (($CH_3)_3COH$, ≥99.7%) were obtained from Fluka. Ethanol (C_2H_6O, ≥99.5%) was obtained from Panreac. Methanol (CH_4O, ≥99.8%), used for HPLC analysis, was obtained from VWR. Ultrapure water was produced in a Direct-Q Millipore system (Merck Millipore, Billerica, MA, USA).

3.2 Catalysts synthesis

The synthesis of g-C_3N_4 was performed by thermal decomposition of dicyandiamide. Briefly, the precursor was placed in a semi-closed crucible inside a muffle furnace under static air conditions. The equipment was programmed to heat at 2 °C min^{-1} ramp up to 450 °C and to maintain that temperature for 2h, followed by heating up to 550 °C and maintain that temperature for 4h. The synthetized material was than rinsed with water to remove any unreacted precursor and dried overnight at 100 °C, Figure 7.
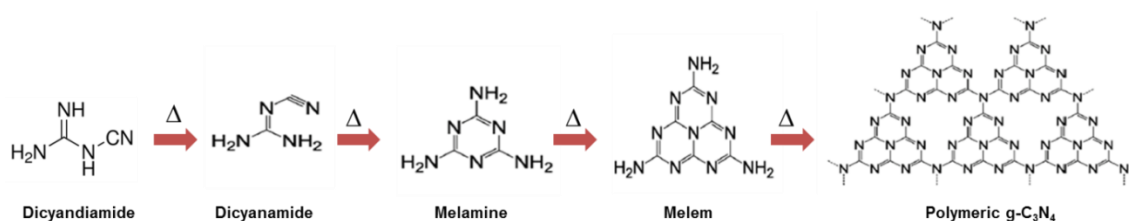
Figure 7 – Production of *bulk* g-C_3N_4 (adapted from [15]).

Thermal exfoliation of g-C_3N_4 was performed by placing a certain amount of *bulk* g-C_3N_4 in a rectangular crucible, which was left in a muffle at 500 °C for 2 h. The final material was labeled as T500, Figure 8.
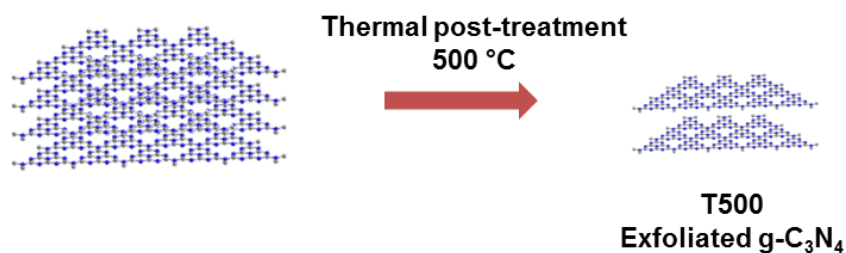
Figure 8 – Production of T500.

As can be observed in, Figure 9, the material presents different color and densities before and after thermal exfoliation.

Figure 9 – The same amount (50 mg) of *bulk* g-C$_3$N$_4$ and after thermal post-treatment (T500).

Magnetic Fe$_3$O$_4$/T500 was produced as follows. T500 (400 mg) were suspended in 250 mL of water and left 1 h under sonication. In a different beaker, 80 mg of FeCl$_2$.4H$_2$O and 234 mg of FeCl$_3$.6H$_2$O were dissolved in 50 mL of water, the final solution being then mixed with the T500 suspension. The misture was heat-treated at 80 ºC for 30 min and then 4 mL of ammonia solution was added and the mixture was left to stir for another 30 min. Finally, the particles were recovered using a magnet, washed until neutral pH of the rinsing water and dried overnight at 100 ºC.

3.3 Catalysts characterization

The synthesized materials were characterized by diffuse reflectance UV-Vis spectrophotometry (DR UV-vis) in a Jasco V-560 spectrometer equipped with an integrating sphere attachment

(Jasco ISV-469). DR UV-vis spectra were recorded in diffuse reflectance mode and converted to equivalent absorption Kubelka–Munk units.

Solid state photoluminescence spectra (PL spectra) were obtained using a spectrofluorometer (Jasco FP-8300) with a 150 W Xenon lamp as light source. Measurements were performed using both excitation and emission bandwidth fixed at 2.5 nm. The excitation wavelength was set at 370 nm and the emission was measured in the 380-700 nm range.The Brunauer-Emmett-Teller (BET) specific surface area (S_{BET}) of the photocatalysts was calculated from N_2 adsorption-desorption isotherms at −196 °C, obtained in a Quantachrome Nova 4200e apparatus.

The morphology of the materials was analysed by scanning electron microscopy (SEM) using a FEI Quanta 400FEG ESEM/EDAX Genesis X4 M instrument. Transmission electron microscopy (TEM) images were obtained using a LEO 906E instrument operating at 120 kV, equipped with a 4 M pixel 28 × 28 mm CCD camera from TRS.

3.4 Point of zero charge

The determination of the pH_{pzc} of the samples was carried out by the following procedure. Initially, it was used 50 mL of a NaCl 0.01 M solution and the pH within each flask was adjusted to a value between 2 and 12 by adding HCl 0.1 M, NaOH 0.1 M or NaOH 0.01 M solutions. Then, 0.15 g of T500 was added to each flask, and the final pH was measured after 48 h under agitation at room temperature. The pH_{pzc} is defined by the point where the curve pH_{final} vs $pH_{initial}$ crosses the line $pH_{final} = pH_{initial}$ [16]. A blank measurement was made without catalyst.

3.5 Photocatalytic experiments

A glass reactor with a maximum capacity of 100 mL was used in photocatalytic experiments, Figure 11 (a). The assays were performed under visible light irradiation using 10 W LEDs with an emission line peaking at 417 nm (FWHM = 17 nm, Figure 10), located symmetrically from the outside at 4.0 cm from the reactor wall. The average nominal irradiance of each vis-LED reaching the reactor was 112.6 mW cm^{-2}.
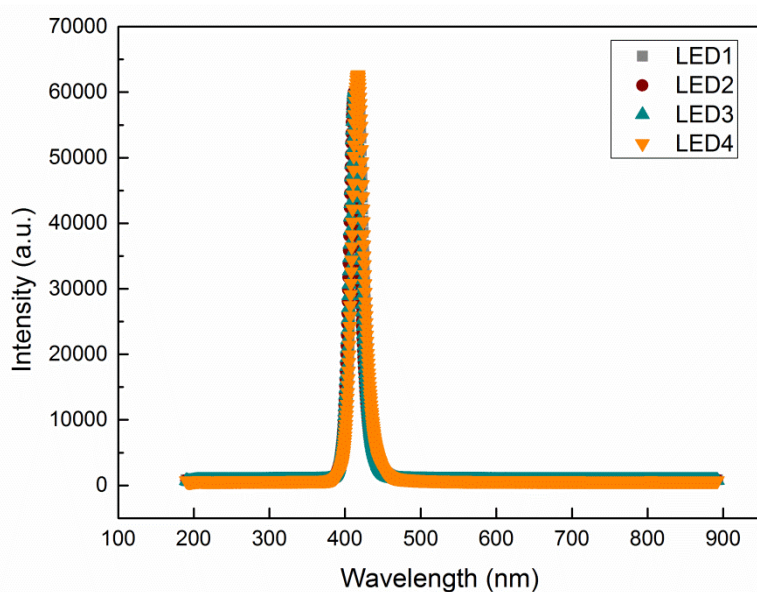
Figure 10 – Spectra of LEDs 417 nm used in this study.

Before irradiation, 50 mL of aqueous suspension containing phenol and the catalyst was stirred in the dark for 15 min before the LEDs were switched on to provide good homogenization of the dispersion and to reach the adsorption-desorption equilibrium in the whole system. During the photocatalytic reaction, air was continuously bubbled through the suspension. The initial concentration of phenol was varied between 20 and 80 mg L^{-1} and the catalyst load was changed from 0.1 to 1.0 g L^{-1}. In a typical experiment, samples were collected at regular times (5, 15, 20, 30, 45, 60, 90 and 120 min), Figure 11 (b). After centrifugation, the liquid samples were analysed by HPLC and UV-vis spectrophotometry for checking the concentration of phenol and H_2O_2, respectively. 0.5 mg of iron(II)-sulfat heptahydrat ($FeSO_4.7H_2O$) was used in Fenton like experiments. In this case, an excess sodium sulfite anhydrous was added to the collected samples. For total organic carbon (TOC) determination, the sample was withdrawn at 120 min.

(a)   **(b)**
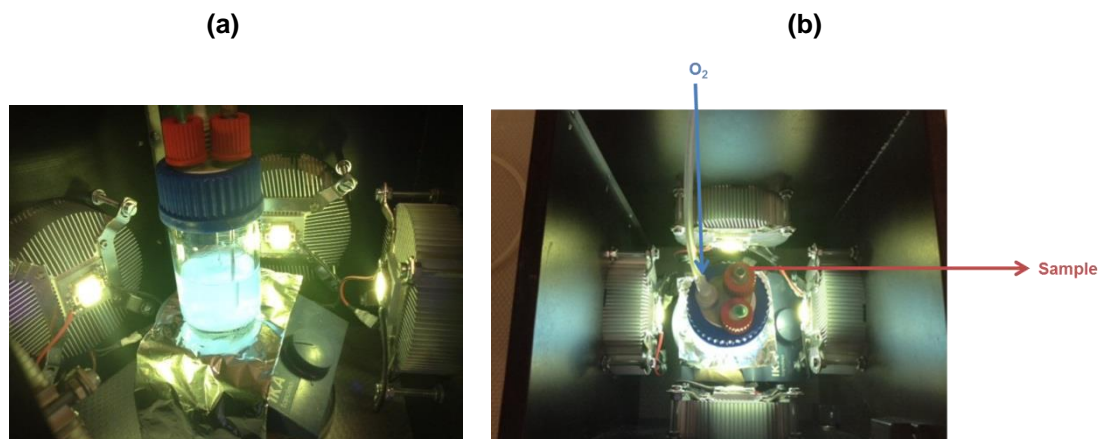
Figure 11 – Photographs of the reaction system (a) top view and (b) lateral view.

3.6 Analytical Methods

In this section are described the equipments and conditions used for product analysis.

3.6.1 High Performance Liquid Chromatography (HPLC)

Samples were withdrawn from the reactor at selected times and the concentration (C) of phenol was determined by high performance liquid chromatography (HPLC) using a Hitachi Elite LaChrom system equipped with a diode array detector (L-2450), a solvent delivery pump (L-2130) and a Purospher Star RP-18 endcapped column (250 mm 4.6 mm, 5 μm particles), using a mobile phase consisting of a mixture water:methanol in a gradient flow. The method started with an equilibrated mixture of water (A):methanol (B) (70:30) at a flow rate of 1 mL min^{-1}, followed by a linear gradient step to A:B (37:63) in 20 min; finally, the initial conditions were re-established in a 1 min gradient step and the A:B (70:30) mixture was isocratically eluted for 7 min. The typical retention time of phenol under these conditions is c.a. 12 min.

3.6.2 Total Organic Carbon (TOC)

The total organic carbon (TOC) content was determined using a Shimadzu TOC-5000A apparatus.

3.6.3 Determination of H_2O_2

For determination of H_2O_2, 300 μL of sample was added to 300 μL of H_2SO_4 and 30 μL of titanium (IV) oxysulfate. The absorbance of the resulting solution was then measured at 405 nm in a JASCO V-560 spectrophotometer.

3.6.4 Kinetic studies

A pseudo-first order reaction kinetic model was used to describe the degradation of phenol:

$$r = \frac{-d[PhOH]}{dt} = k_{app}[PhOH] \qquad (8)$$

where [PhOH] corresponds to the phenol concentration, k_{app} is the apparent first order reaction kinetic constant and t is the reaction time. The integration of Equation 9 gives:

$$\frac{[PhOH]}{[PhOH]_0} = e^{-k_{app}t} \qquad (9)$$

where $[PhOH]_0$ is the phenol concentration for $t = 0$. The values of $k_{app,}$ for the photocatalytic reactions were obtained by non-linear fitting of Equation 9 to the experimental data. No degradation of phenol was observed under dark conditions.

4 Results and discussion

Different parameters such as pH, light intensity, initial concentration of target compounds and photocatalyst load were studied for phenol degradation and H_2O_2 production. The following section will provide these results.

4.1 Catalysts characterization

The *bulk* g-C_3N_4 and T500 materials were characterized by PL spectroscopy, under an excitation energy fixed a 370 nm, Figure 12. The spectrum of T500 shows an increase of the PL peak intensity. Compared with *bulk* g-C_3N_4, the emission peak of the nanosheets shifts from 450 to 490 nm. Correspondingly, the intrinsic absorption edge of g-C_3N_4 nanosheets also exhibits blue-shift in comparison with bulk g-C_3N_4, with the bandgap increasing from 2.57 eV of the *bulk* one to 2.75 eV of the nanosheets. The larger bandgap and blue-shift of fluorescence peaks can be attributed to the quantum confinement effect, due to the lower dimensions of T500 particles [17].
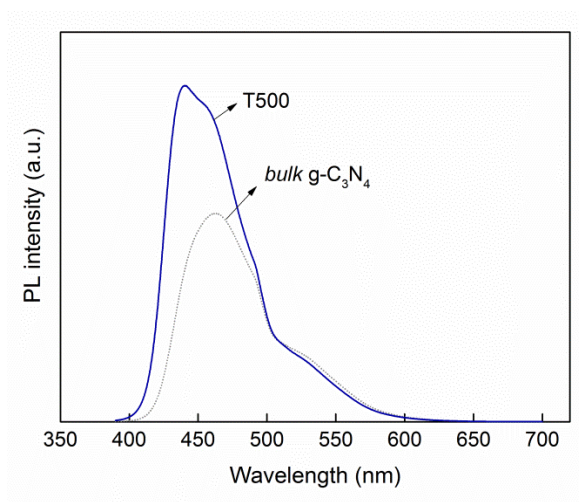
Figure 12 – Solid state photoluminescence (PL) spectra for *bulk* g-C_3N_4 and T500.

C_3N_4-based photocatalysts can be designed to drive various reduction and oxidation reactions under light irradiation with suitable wavelengths (up to 460 nm). As represented in Figure 13 these materials possess extended absorption to the visible, when compared to TiO_2, which only absorbs until 400 nm, *i.e.,* in the UV spectral region.
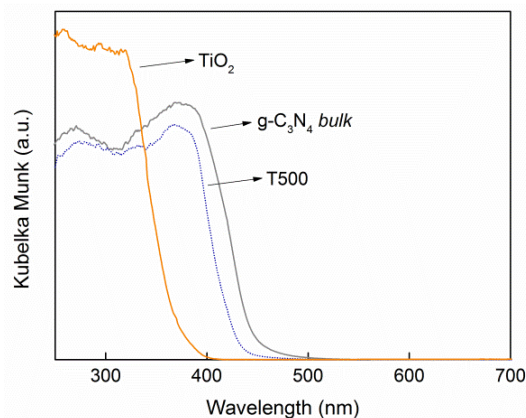
Figure 13 – DRUV-vis of *bulk* g-C$_3$N$_4$, T500 and TiO$_2$ catalysts.

TEM analysis of TiO$_2$ Evonik P25 reveals the presence of crystallites of dimensions varying between 20 and 30 nm, Figure 14 (a), which aggregate as bigger particles, as can be confirmed by SEM, Figure 14 (b). This material is constituted by 80% anatase and 20% rutile crystalline phases and possesses a specific surface area of ca. 50 m^2 g^{-1} [18].

(a)   **(b)**
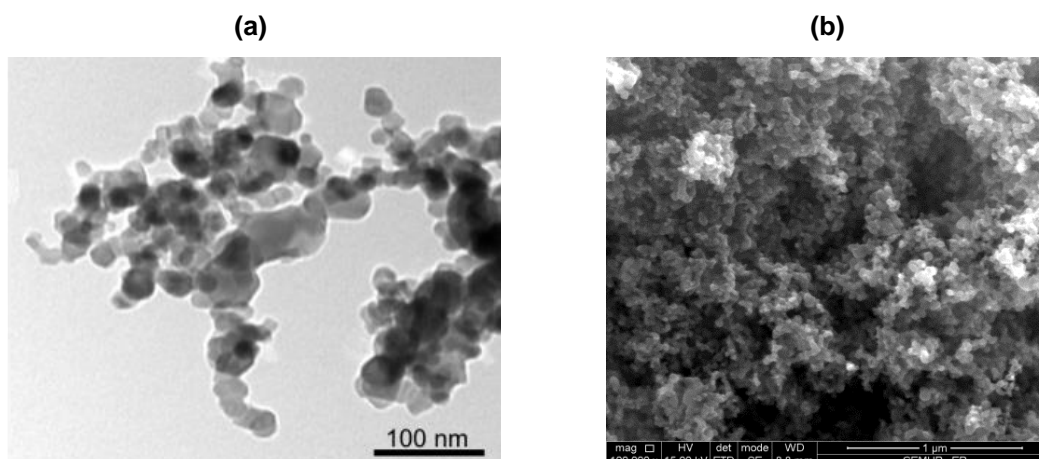
Figure 14 – TEM (a) and SEM (b) micrographs of TiO$_2$.

It was found that exfoliating *bulk* g-C$_3$N$_4$ into ultra-thin two-dimensional g-C$_3$N$_4$ nanosheets is an effective strategy to enhance its photocatalytic efficiency [19]. Two SEM images of these two materials are shown in Figure 15. In the *bulk* material, the layers are more close to each other (darker image) and the BET surface area is lower, S$_{BET}$ = 5 m^2 g^{-1} while in the T500 sample layers are away from each other and the BET surface area is much higher, S$_{BET}$ = 87 m^2 g^{-1}. The higher specific surface area of T500 may indicate a higher accessibility of surface active sites and make charge carriers transport easier, eventually leading to an enhancement of the photocatalytic performance.

(a)   **(b)**
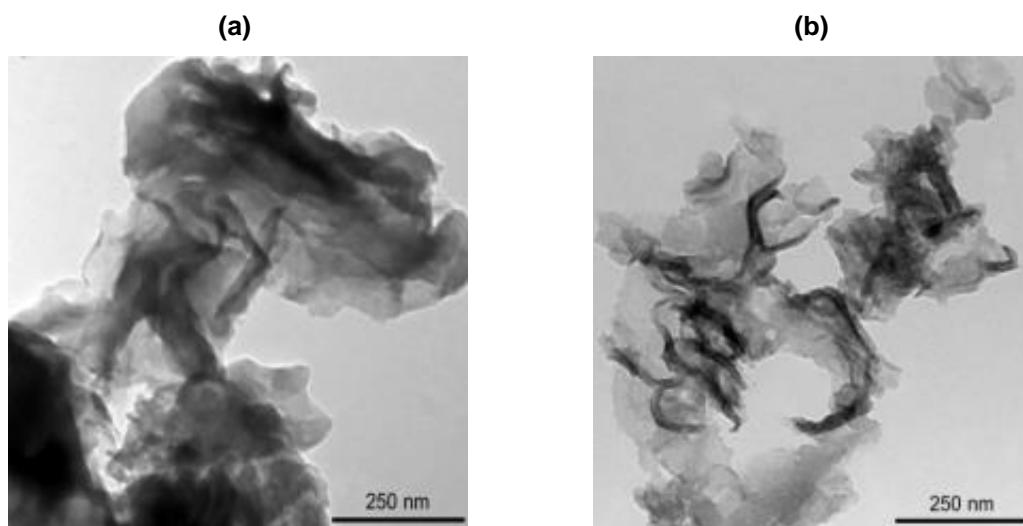
Figure 15 – SEM micrographs of *bulk* g-C$_3$N$_4$ (a) and T500 (b).

The performance of the carbon materials in catalysis depends on their surface properties, which depends on materials structure. One parameter that is quite useful for a global description of the surface chemistry of carbon materials is the point of zero charge. To analyse this parameter, carbon materials are suspended in aqueous acidic and basic solutions. Acidic groups tend to dissociate, giving protons to the solution and leaving the carbon surface negatively charged, while basic groups tend to attract protons from the solution and the surface becomes positively charged. The net surface charge will be zero at some specific value of pH and this is the point of zero charge (PZC). So when pH>pH$_{PZC}$, the surface is negatively charged due to the deprotonated acid groups and will attract cations. If the surface is positively charged, pH<pH$_{PZC}$, as a result of protonated basic sites, anions will be attracted [20]. The PZC of T500 is situated between pH 2 and 3, Figure 16, meaning that this material possesses an acidic surface, which is due to the equilibrium of chemical reactions between hydrogen ions, hydroxyl ions, and amine groups on the g-C$_3$N$_4$ surface [21]. Thus, above the pH value of 3 until neutral pH the catalyst will not repulse the phenol molecules since the respective p*Ka* of phenol is near 10 (i.e. phenol molecules are protonated below pH 10).
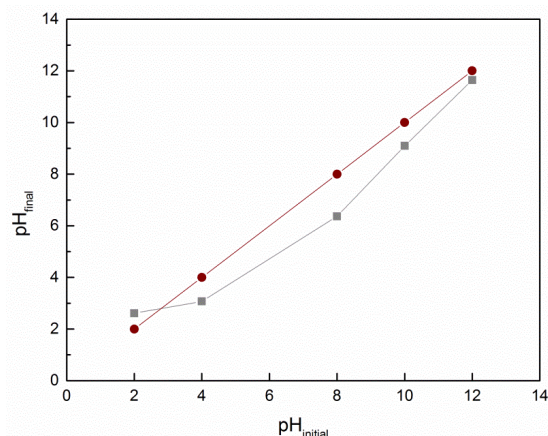
Figure 16 – Determination of the point of zero charge of T500.

4.2 Photocatalytic degradation of phenol

Experiments performed with an initial phenol concentration of 20 ppm and 1 g L^{-1} of catalyst, Figure 17 and Table 1, show that T500 can remove phenol faster than the other catalysts tested. In comparison with TiO_2-P25, these results were expected since the absorption band of T500 is clearly in the visible region of the spectrum, Figure 13, and it needs less energy for charge excitation (2.7 eV), comparatively with TiO_2-P25 (3.2 eV). The removal of phenol was lower with *bulk* g-C_3N_4, revealing that exfoliation has a strong positive impact on the phenol removal.
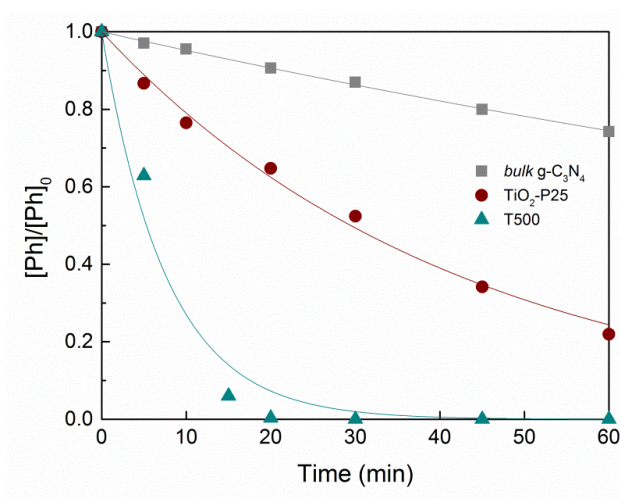
Figure 17 – Normalized phenol concentration in photocatalytic experiments using different catalysts (catalyst load: 1.0 g L^{-1} and initial phenol concentration: 20 ppm).

Table 1 – Kinetic constants for different catalysts.

Catalyst	k_{app} ($\times 10^{-2}$) (min^{-1})
bulk g-C_3N_4	0.49
TiO_2-P25	2.35
T500	13.09

4.3 Influence of operating parameters on the photocatalytic degradation of phenol

Two different concentrations of phenol were tested (20 and 50 ppm) and the experiments compared with UP H_2O only regarding the H_2O_2 production, Figure 18. It is possible to observe that the concentration of H_2O_2 is residual in UP H_2O and quite high when using phenol (the H_2O_2 concentration increasing with that of phenol).
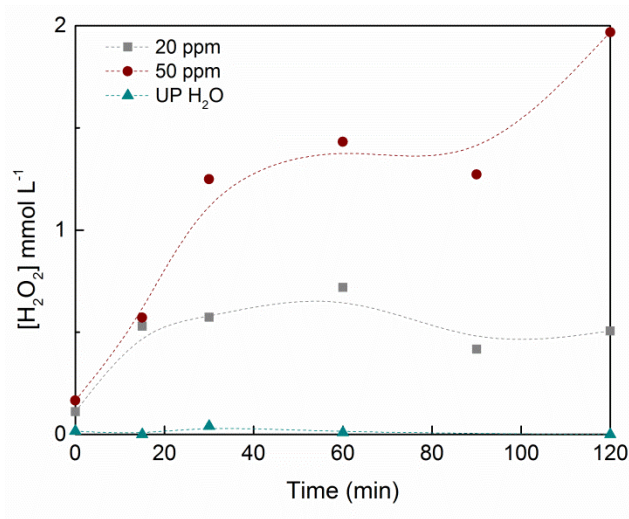
Figure 18 – Concentration evolution of H_2O_2 using UP H_2O and two different concentrations of phenol (catalyst load: 0.5 g L^{-1}).

4.4 Effect of photocatalyst load

Experiments performed at different photocatalyst loads (0.1 - 1.0 g L^{-1}) show that the H_2O_2 concentration produced is the highest at 0.25 g L^{-1} of T500, Figure 19 (a). The removal of phenol, Figure 19 (b) and Table 2, is quite similar above 0.25 g L^{-1} of T500, but faster at 0.75 g L^{-1}, Table 2. However, the highest TOC removal (51 %) was achieved using 0.25 g L^{-1} of catalyst, Figure 20. Thus, a catalyst load of 0.5 g L^{-1} was selected for next studies, also because it is used as typical load in photocatalytic experiments.
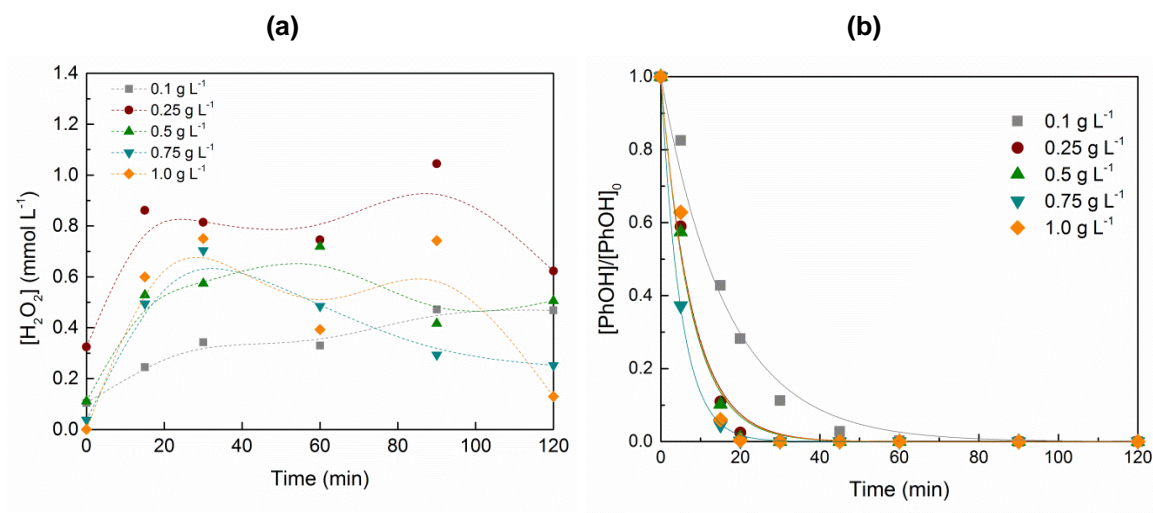
Figure 19 – (a) Concentration evolution of H_2O_2 and (b) normalized phenol concentration using different catalyst loads (initial phenol concentration: 20 ppm).

Table 2 – Kinetic constants using different catalyst loads.

Catalyst load (g L^{-1})	k_{app} (x10^{-2}) (min^{-1})
0.1	6.08
0.25	12.88
0.5	13.35
0.75	20.06
1.0	13.09
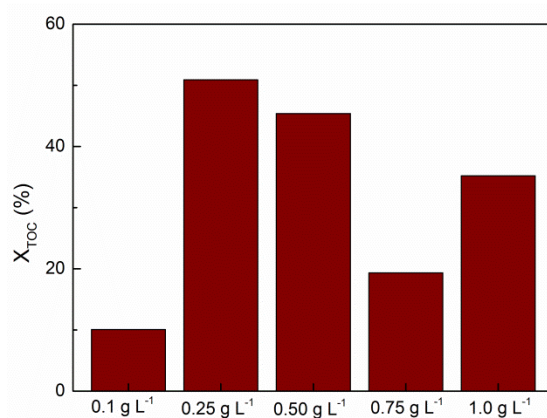
Figure 20 – X_{TOC} for the different catalyst loads with a phenol concentration of 20 ppm.

4.5 Effect of initial phenol concentration

Different initial phenol concentrations were studied (20 – 80 ppm) in the experiments with T500, Figure 21 and Table 3.
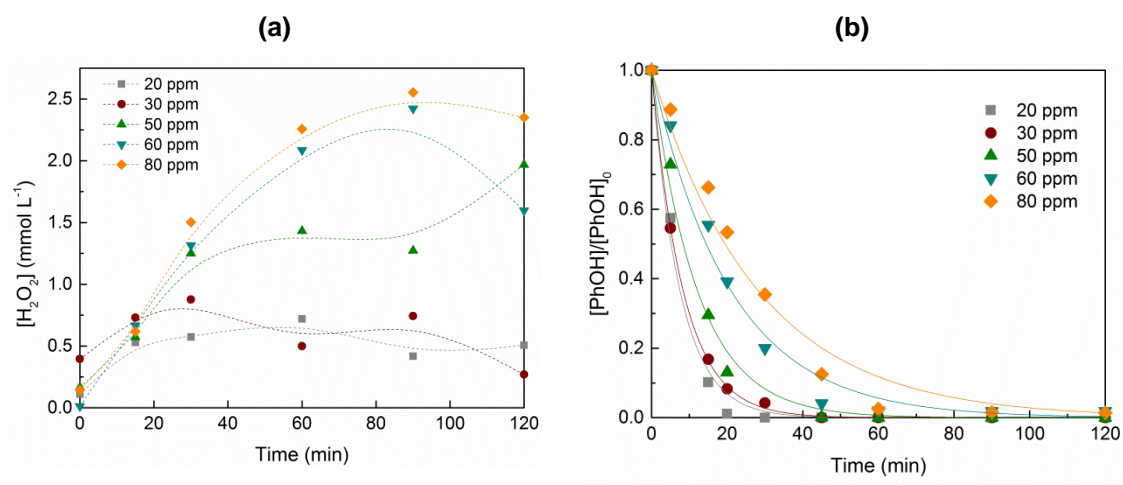
Figure 21 – (a) Concentration evolution of H_2O_2 and (b) normalized phenol concentration using different initial phenol concentrations (catalyst load: 0.5 g L^{-1}).

In all the cases, phenol is degraded to values below the detection limits in 60 min Figure 21 (b). It is interesting to observe that the amount of H_2O_2 increases with the phenol concentration used, suggesting that phenol is acting as a scavenger of holes and more H_2O_2 is produced, Figure 4.

Table 3 – Kinetic constants using different initial phenol concentrations.

Phenol concentration (ppm)	k_{app} ($\times 10^{-2}$) (min^{-1})
20	13.35
30	12.03
50	8.29
60	4.79
80	4.79

Regarding the TOC removal, Figure 22, it seems to increase with the phenol concentration, except for 30 ppm of phenol, TOC removals of 75 % and 74 % being achieved for initial phenol concentrations of 30 and 80 ppm, respectively.
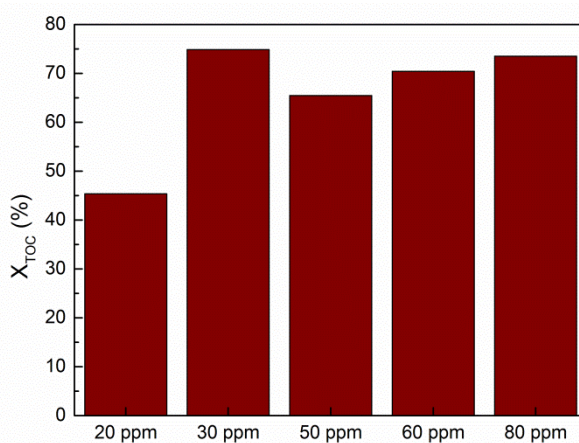
Figure 22 – X_{TOC} for experiments performed with different initial phenol concentrations.

4.6 Addition of H_2O_2 in the initial solution

This study was performed in the absence of catalyst, adding ca. 2.0 mmol L^{-1} of H_2O_2 to the initial phenol solution. It is possible to conclude that phenol was not degraded Figure 23 (b) and Table 4 and the H_2O_2 concentration was practically similar during the experiment Figure 23 (a) the value shown for $t = 0$ min being that determined for the sample analysed just before adding H_2O_2, but slightly lower than the expected one. The observed deviations may be related with some experimental errors. In fact, one of the suggestions for future work is to repeat the significant experiments of this dissertation, at least in triplicate, for determination of all the experimental errors.

(a)   **(b)**
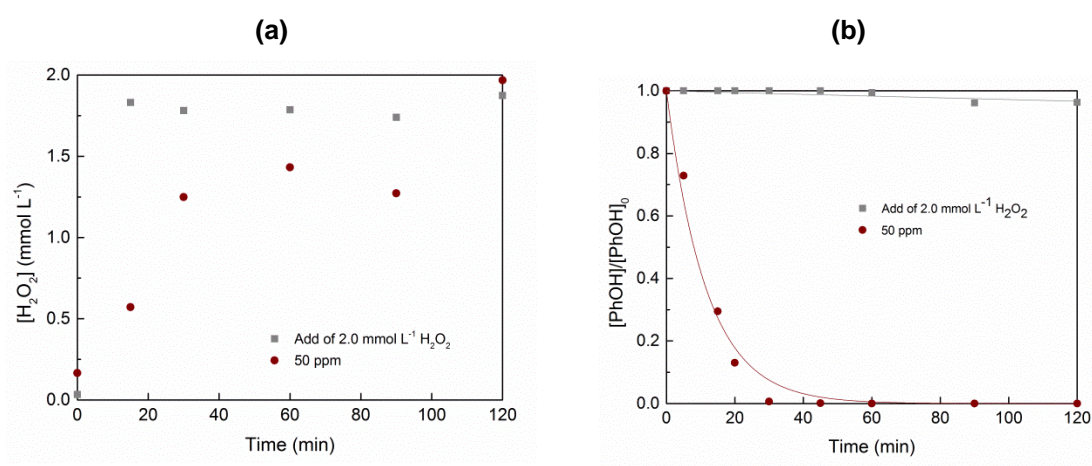
Figure 23 – (a) Concentration of H_2O_2 and (b) normalized phenol concentration adding H_2O_2 (2.0 mmol L^{-1}) to the initial phenol solution of 50 ppm (without catalyst). The results obtained in the presence of T500 (without adding H_2O_2) are also included for comparison purposes.

Table 4 – Kinetic constants for the experiments with T500 or adding H_2O_2 (2.0 mmol L^{-1}).

Experiment	k_{app} (x10^{-2}) (min^{-1})
With T500 and without add H_2O_2	8.63
Without T500 and add 2.0 mmol L^{-1} of H_2O_2	0.03

4.7 Effect of different light sources

The phenol removal is slower when using LEDs of 370 nm than when using those of 417 nm, Figure 24 (b) and Table 5, in the absence or presence of Fe species, whereas the H_2O_2 concentration tends to increase until 90 min for all the studied conditions, Figure 24 (a).

(a) **(b)**
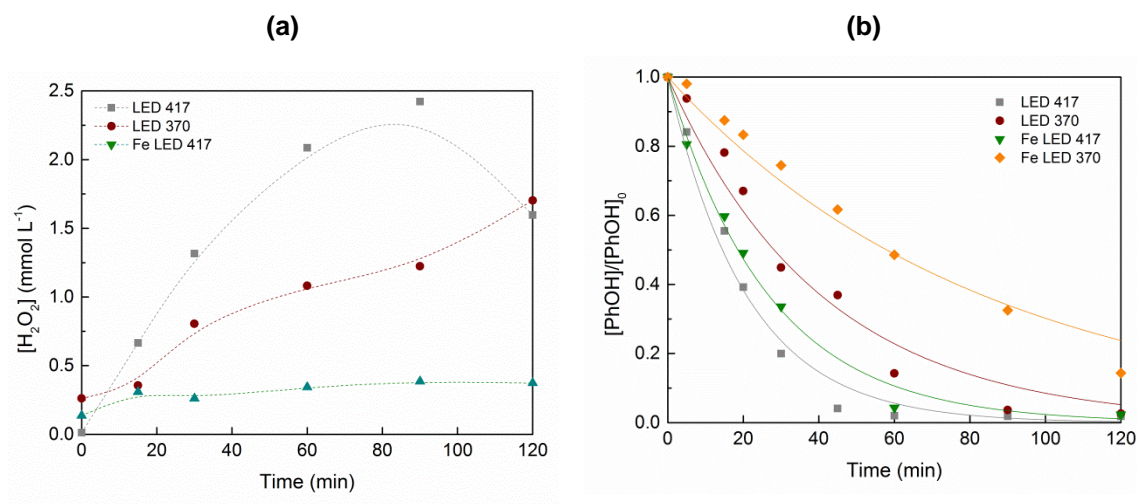
Figure 24 – (a) Concentration evolution of H_2O_2 and (b) normalized phenol concentration using different radiation sources and 60 ppm of initial phenol concentration (catalyst load: 0.5 g L^{-1}).

Table 5 – Kinetic constants for different types of radiation sources.

Experiment	k_{app} (x10^{-2}) (min^{-1})
LED 417	4.79
LED 370	2.46
Fe LED 417	3.74
Fe LED 370	1.20

The same trend was observed for the TOC removals, lower for UV LED (45 %) than when using visible LED (70 %) in the absence of Fe, as also observed in the presence of Fe species.
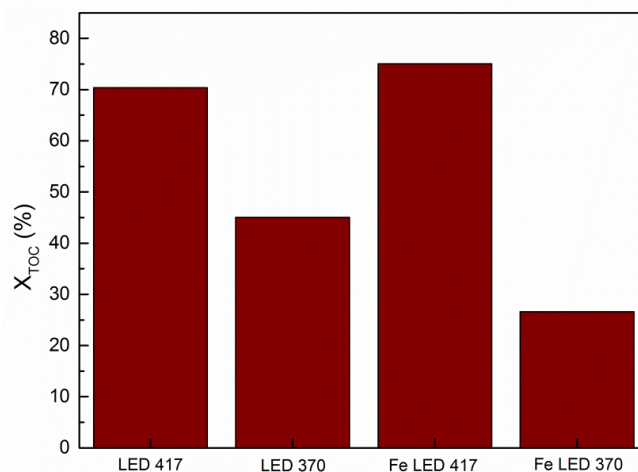
Figure 25 – X_{TOC} for the experiments using LED 417 and LED 370 with and without Fe species.

4.8 Effect of radical and hole scavengers

TEOA, Triethanolamine, is a hole scavenger while *t*-BuOH is a radical scavenger. The H_2O_2 concentration is higher Figure 26 (a) when using TEOA because the holes are occupied with TEOA, avoiding the electron/hole recombination and increasing the H_2O_2 generation. In contrast, the phenol removal is less efficient, Figure 26 (b) and Table 6, demonstrating that phenol is degraded by means of the photogenerated holes. Using *t*-BuOH, the concentration of H_2O_2 is much lower because there are less electrons available and phenol removal slow down because *t*-BuOH consumes the hydroxyl radicals, Figure 26 (b).

(a) **(b)**
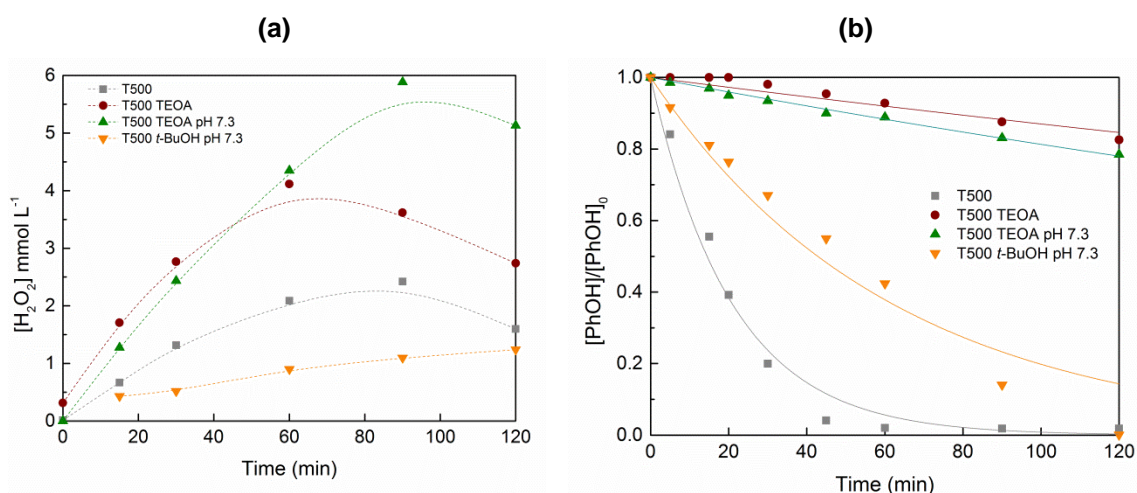
Figure 26 – (a) Concentration evolution of H_2O_2 and (b) normalized phenol concentration using an initial phenol concentration of 60 ppm and adding TEOA and *t*-BuOH to the initial solution (catalyst load: 0.5 g L^{-1}).

Table 6 – Kinetic constants using scavengers.

Experiment	k_{app} (x10^{-2}) (min^{-1})
T500	4.79
T500 TEOA	0.14
T500 TEOA pH 7.3	0.21
T500 *t*-BuOH pH 7.3	1.62

4.9 Photo-Fenton like experiments

As discussed above, H_2O_2 is one of the by-products of the degradation of phenol using T500 irradiated in the visible range. If iron species are added to the solution, photo-Fenton reaction can take place. The advantage is that in this case there is no need to add H_2O_2 to the system because it is produced *in-situ*. It is already known that photo-Fenton reaction perform better at acidic pH between 2 and 3.

When Fe specied were added to the reaction medium at natural pH, there was a decrease in the k_{aap} comparing to the reaction with only T500. On the other hand, lowering the pH of the suspension to c.a. 2.7, an increase in the rate of phenol degradation was observed in Figure 27 (b) and Table 7. At the same time, under these conditions, the concentration of H_2O_2 present in solution decreased, Figure 27 (a), which indicates that it is being converted to hydroxyl radicals through a photo-Fenton route. These hydroxyl radicals will attack the aromatic ring of the phenol molecules increasing the efficiency of the degradation process.
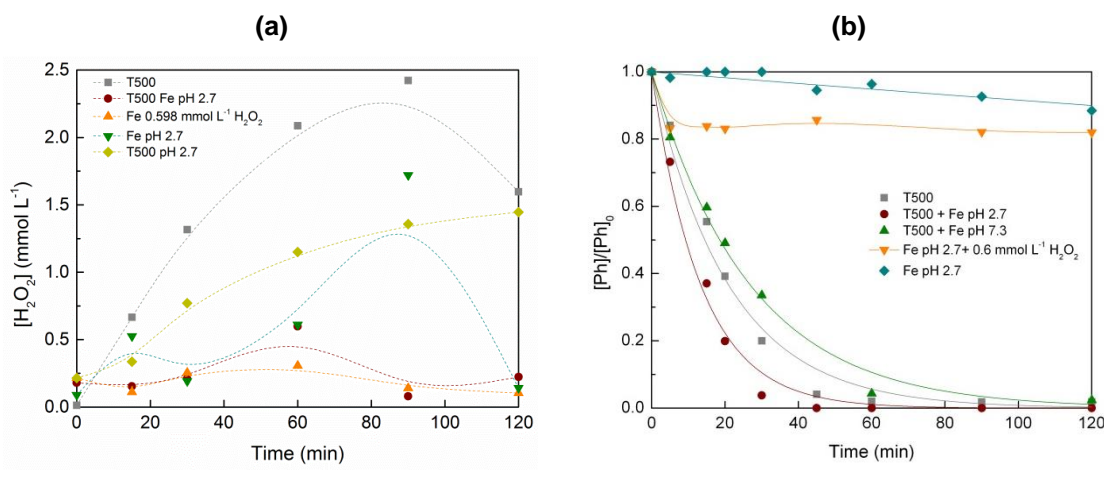
Figure 27 – (a) Concentration evolution of H_2O_2 and (b) normalized phenol concentration using different experimental conditions and adding Fe to the phenol initial solution of 60 ppm (catalyst load: 0.5 g L^{-1}).

Table 7 – Kinetic constants for different experimental conditions with and without Fe species in the initial solution.

Experiment	k_{app} (x10^{-2}) (min^{-1})
T500	4.79
T500 Fe pH 2.7	7.50
T500 Fe pH 7.3	3.74
Fe 0.598 mmol L^{-1} H_2O_2	0.23
Fe pH 2.7	n.a.

Although the the adition of Fe species in homogeneous photo-Fenton processes has proved to be highly efficient for the degradation of several pollutants, there are several concerns when using iron salts as source of Fe^{2+} for the treatment of wastewaters, such as the generation of sludge wastes when the pH is increased after the treatment to precipitate the iron species. Iron-based heterogeneous catalysts have been the focus of several studies in the recent years since it avoids the presence of high concentrations of iron species in the treated waters (the European Union standards for discharge of treated waters being 2.0 mg Fe L^{-1}), the loss of catalyst, as well as the sludge produced in the homogeneous process. The resulting system is known as photo-Fenton-like process (or heterogeneous photo-Fenton process).

In this work we used magnetic Fe_3O_4/T500 as catalysts of the photo-Fenton-like degradation of phenol, Figure 28 (b) and Table 8. It was observed a decrease in the photo efficiency of the process under both acidic and natural pH conditions, probably due to a too higher fraction of the surface of T500 that became inaccessible to phenol because of the presence of Fe_3O_4 particles. Although the synthesis of this material has to be optimized in further studies, the main

advantage is that in slurry operation, the catalyst can be easily separated from the treated water by an external magnetic field.

(a)

(b)
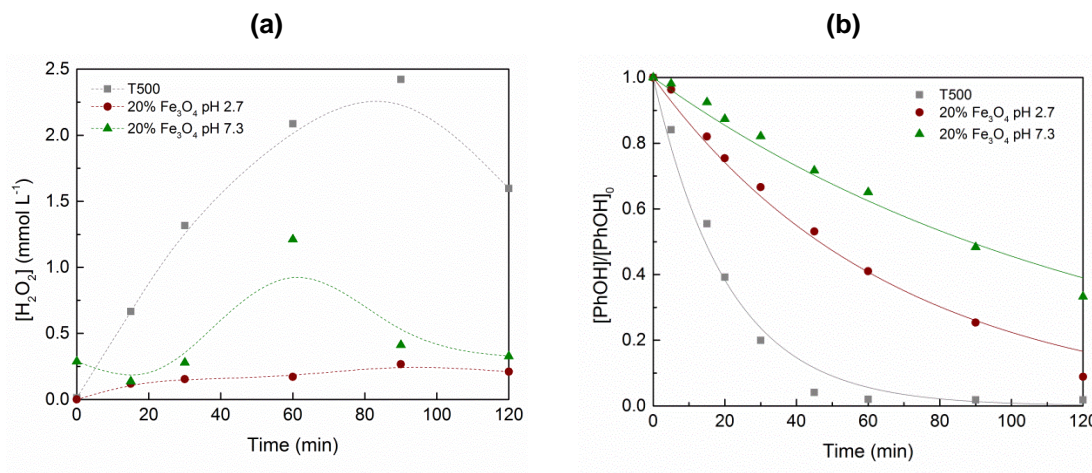
Figure 28 – (a) Concentration evolution of H_2O_2 and (b) Normalized phenol concentration using 20 % of Fe_3O_4 and an initial phenol solution of 60 ppm (catalyst load: 0.5 g L^{-1}).

Table 8 – Kinetic constants with 20 % of Fe_3O_4.

Experiment	k_{app} (x10^{-2}) (min^{-1})
T500	4.79
20% Fe_3O_4 pH 2.7	1.50
20% Fe_3O_4 pH 7.3	0.79
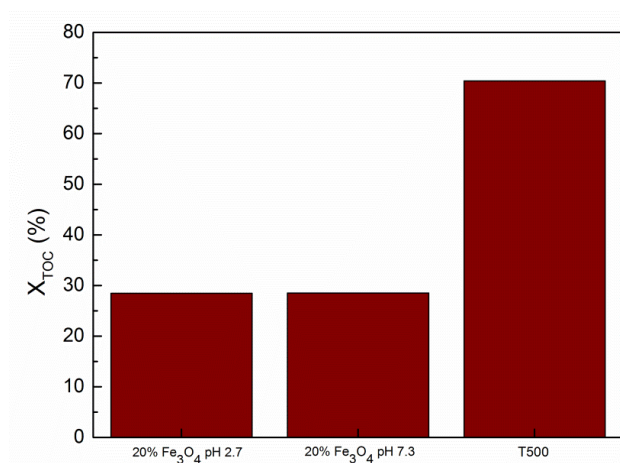
Figure 29 – X_{TOC} using 20% of Fe_3O_4 and an initial phenol solution of 60 ppm (catalyst load: 0.5 g L^{-1}).

4.10 Effect of the temperature with T500 and Fe species

Using the natural pH of 7.3 there is production of hydroxly radicals when the temperature increase so the degradation of phenol was more efficient, Figure 30 (b) and Table 9. Although the TOC, Figure 31, was lower so there was more production of by-products.

(a) **(b)**
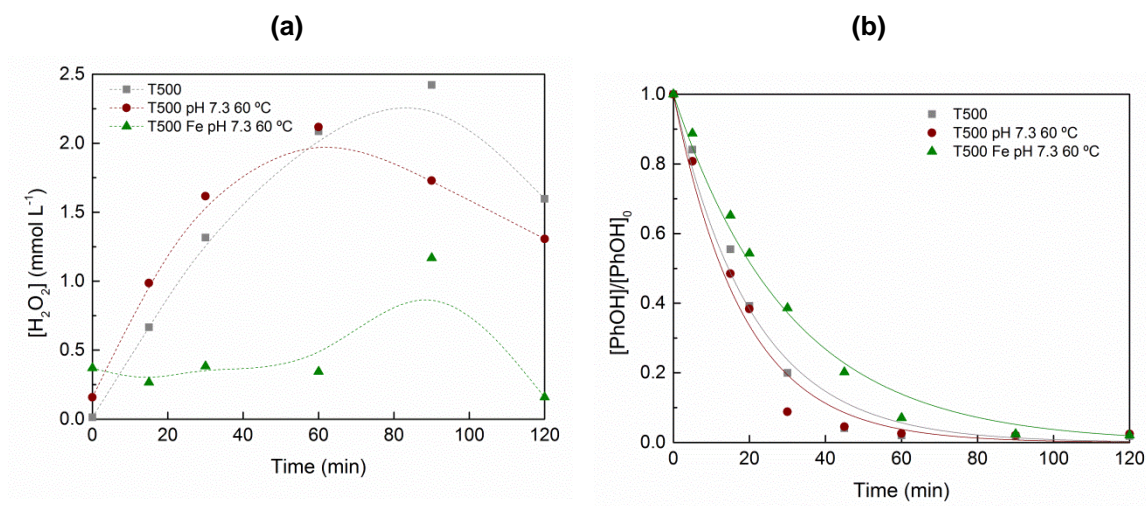
Figure 30 – (a) Concentration evolution of H_2O_2 and (b) normalized phenol concentration using 60 °C and an initial phenol solution of 60 ppm (catalyst load: 0.5 g L^{-1}).

Table 9 – Kinetic constants using different conditions (presence of Fe) at 60 °C.

Experiment	k_{app} (x10^{-2}) (min^{-1})
T500	4.79
T500 pH 7.3 60 °C	5.46
T500 Fe pH 7.3 60 °C	3.29
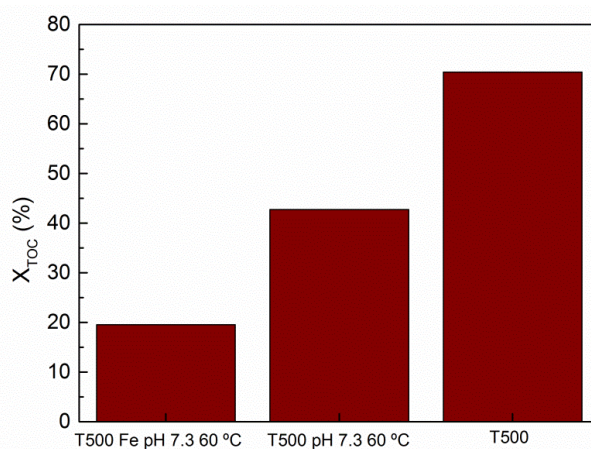
Figure 31 – X_{TOC} using different conditions and an initial phenol solution of 60 ppm (catalyst load: 0.5 g L^{-1}).

The phenol removal decreases by increasing the temperature, Figure 32 (b) and Table 10, probably due to the H_2O_2 decomposition to oxygen and water rather than to hydroxyl radicals. However, the H_2O_2 concentration is lower in 60 min at 60 °C and in 90 min at 20 °C, Figure 32 (a); thus, more studies are needed to better understand the temperature effect on the H_2O_2 concentration. Regarding the TOC removal, Figure 33, it is higher (85 %) for the highest temperature tested (60 ⁰C), but lower at 40 ⁰C rather than at 20 ⁰C.
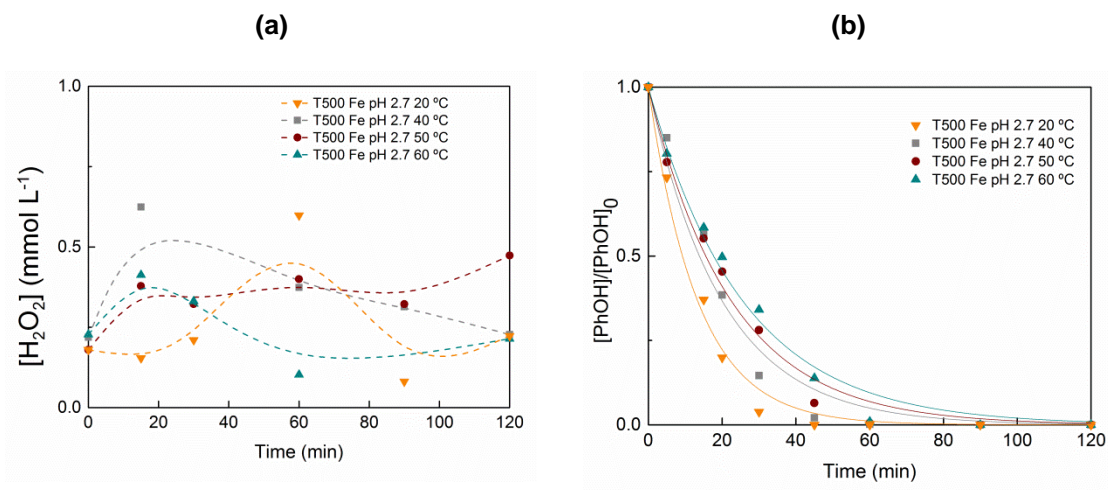
Figure 32 – (a) Concentration evolution of H_2O_2 and (b) normalized phenol concentration using different temperatures and an initial phenol solution of 60 ppm (catalyst load: 0.5 g L^{-1}).

Table 10 – Kinetic constants using different temperatures.

Temperature (°C)	k_{app} (x10^{-2}) (min^{-1})
20	7.50
40	5.01
50	4.46
60	3.92
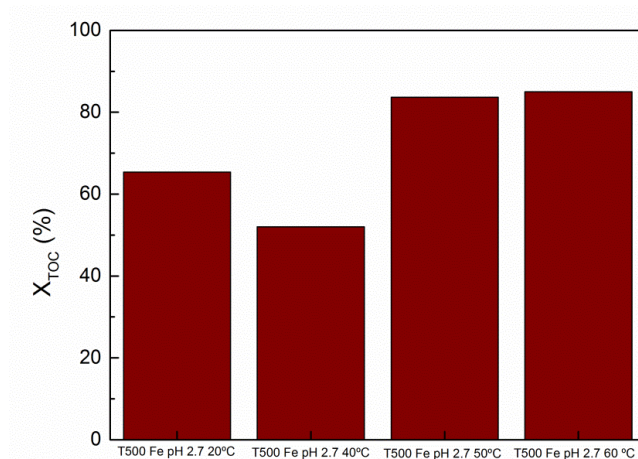
Figure 33 – X_{TOC} using different temperatures and an initial phenol solution of 60 ppm and a catalyst load of 0.5 g L^{-1}.

4.11 By-products

In the reactions studied catechol was not detected. Two phenol by-products (benzoquinone and hydroquinone) were detected in the experiments using T500 and TiO_2-P25, while benzoquinone was the only by-product detected with *bulk* g-C_3N_4, Figures 34 (a) and 34 (b). In the photo-Fenton experiment there were no by-products to be detected, probably due to the highly efficiency of this process for the degradation of not only phenol but also its intermediates.

(a)   **(b)**
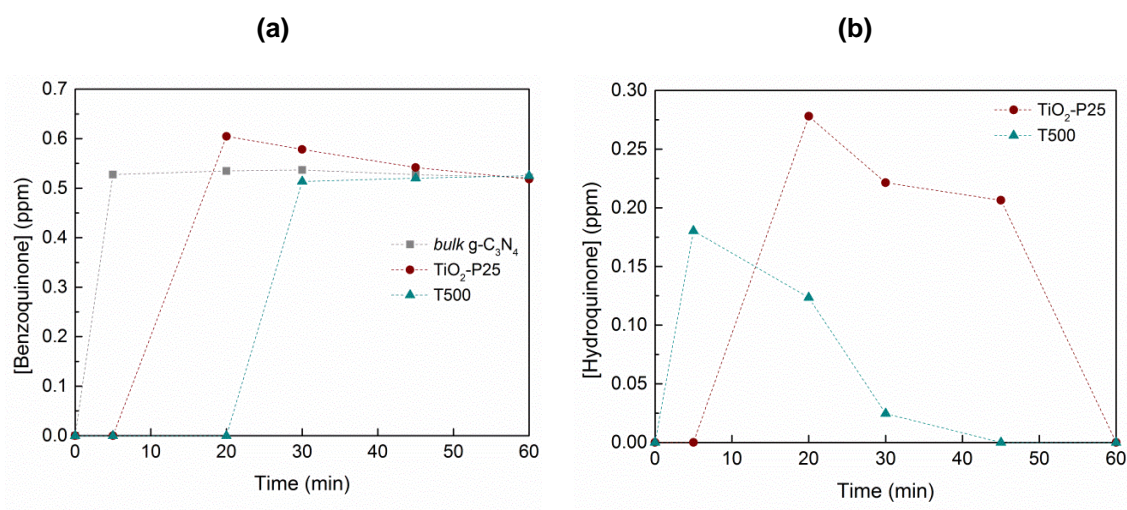
Figure 34 – (a) Benzoquinone and (b) hydroquinone concentrations using *bulk* g-C_3N_4, TiO_2-P25 and T500 with an initial phenol concentration of 20 ppm.

5 Conclusion

● The thermal treatment of the *bulk* g-C_3N_4 at 500 °C produced an exfoliated sample of the material. The BET surface area of the exfoliated g-C_3N_4 was found to increase to 87 $m^2 g^{-1}$.

● The photocatalytic degradation of phenol was more efficient with T500 and it was observed that using this photocatalyst, a simultaneous production of H_2O_2 was occurring concomitant to phenol removal from the solution.

● Using selective scavangers led to the conclusion that the photocatalytic mechanism operative in this case, was generating H_2O_2 through the reductive electrons of the conductive band (CV) while the degradation of phenol was taking place in the holes of g-C_3N_4 surface. Additionally the presence of oxygen reactive species, such as $HO^•$ could also promote the phenol degradation.

● The g-C_3N_4 treated at 500 °C (T500) can remove phenol faster than the benchmark photocatalyst (TiO$_4$-P25).

● Adding iron to the system increased the removal of phenol, by a Photo-Fenton like process.

● At higher temperatures the photocatalytic degradation of phenol was less efficient because H_2O_2 was degraded (so there was no additional production of $HO^•$ radical) and desorption is known to increase with increasing temperature.

● In the presence of Fe_3O_4/T500 the efficiency of phenol degradation decreased, which can be attributed to a high fraction of T500 surface that is occupied by Fe_3O_4 particles and that is unavaulable for phenol degradation. Nevertheless, this material can be easily separated from the treated water by using an external magnetic field.

6 Assessment of the work done

6.1 Outputs of the described work

A.R. Morgado*, M.J. Lima, M.J. Sampaio, C.G. Silva, J.L. Faria, A.M.T. Silva, "Graphitic carbon nitride as photocatalyst for phenol degradation using visible light", I Reunião do Grupo do Carbono da Sociedade Portuguesa de Química, Porto (Portugal), June 2017 (Poster Communication).

A.R. Morgado*, M.J. Lima, M.J. Sampaio, C.G. Silva, J.L. Faria, A.M.T. Silva, "Effective visible light phenol degradation using photocatalytically active carbon nitride nanosheets", DCE 2017 – Doctoral Congress in Engineering 2017, Porto (Portugal), June 2017 (Oral Communication).

6.2 Future Work

It would be interesting to study the possibility of modification the material introducing particles of Fe on the surface of $g\text{-}C_3N_4$, aiming to improve the photo-Fenton mechanism. This modification will probably increase the surface area of $g\text{-}C_3N_4$. Additionally, the use of magnetic particles will potentiate the separation of the photocatalyst without using centrifugation process.

The next logical step is to move to real case pollutants, like other phenol derivatives, or even other compounds, who are difficult to convert or mineralize by using conventional processes, such as carbamazepine.

One interesting option would be to study a real industry wastewater, in the presence of T500.

Improving the production of H_2O_2 from ultrapure H_2O could pave the way to develop alternative methods for the production of this commodity.

Induce modifications in $g\text{-}C_3N_4$ surface with the aim of changing the oxidation potential of the surface could expand the possibilities of the material.

References

1.	Lima, M.J., Leblebici, M.E., Dias, M.M., Lopes, J.C., Silva, C.G., Silva, A.M., and Faria, J.L., *Continuous flow photo-Fenton treatment of ciprofloxacin in aqueous solutions using homogeneous and magnetically recoverable catalysts.* Environ Sci Pollut Res Int, 2014. **21**(19): p. 11116-25.

2.	Armaroli, N. and Balzani, V., *The future of energy supply: Challenges and opportunities.* Angew Chem Int Ed Engl, 2007. **46**(1-2): p. 52-66.

3.	Lima, M.J., Tavares, P.B., Silva, A.M.T., Silva, C.G., and Faria, J.L., *Selective photocatalytic oxidation of benzyl alcohol to benzaldehyde by using metal-loaded g-C 3 N 4 photocatalysts.* Catalysis Today, 2017. **287**: p. 70-77.

4.	Wen, J., Xie, J., Chen, X., and Li, X., *A review on g-C3N4-based photocatalysts.* Applied Surface Science, 2017. **391**: p. 72-123.

5.	Chiou, C.-H., Wu, C.-Y., and Juang, R.-S., *Influence of operating parameters on photocatalytic degradation of phenol in UV/TiO2 process.* Chemical Engineering Journal, 2008. **139**(2): p. 322-329.

6.	Mamba, G. and Mishra, A.K., *Graphitic carbon nitride (g-C3N4) nanocomposites: A new and exciting generation of visible light driven photocatalysts for environmental pollution remediation.* Applied Catalysis B: Environmental, 2016. **198**: p. 347-377.

7.	Li, X., Yu, J., and Jaroniec, M., *Hierarchical photocatalysts.* Chem Soc Rev, 2016. **45**(9): p. 2603-36.

8.	Tamirat, A.G., Rick, J., Dubale, A.A., Su, W.-N., and Hwang, B.-J., *Using hematite for photoelectrochemical water splitting: a review of current progress and challenges.* Nanoscale Horiz., 2016. **1**(4): p. 243-267.

9.	Cui, Y., Ding, Z., Liu, P., Antonietti, M., Fu, X., and Wang, X., *Metal-free activation of H2O2 by g-C3N4 under visible light irradiation for the degradation of organic pollutants.* Phys Chem Chem Phys, 2012. **14**(4): p. 1455-62.

10.	Sampaio, M.J., Silva, C.G., Silva, A.M.T., Vilar, V.J.P., Boaventura, R.A.R., and Faria, J.L., *Photocatalytic activity of TiO2-coated glass raschig rings on the degradation of phenolic derivatives under simulated solar light irradiation.* Chemical Engineering Journal, 2013. **224**: p. 32-38.

11.	Kofuji, Y., Isobe, Y., Shiraishi, Y., Sakamoto, H., Tanaka, S., Ichikawa, S., and Hirai, T., *Carbon Nitride-Aromatic Diimide-Graphene Nanohybrids: Metal-Free Photocatalysts for Solar-to-Hydrogen Peroxide Energy Conversion with 0.2% Efficiency.* J Am Chem Soc, 2016. **138**(31): p. 10019-25.

12.	Zhang, H., Guo, L.H., Zhao, L., Wan, B., and Yang, Y., *Switching Oxygen Reduction Pathway by Exfoliating Graphitic Carbon Nitride for Enhanced Photocatalytic Phenol Degradation.* J Phys Chem Lett, 2015. **6**(6): p. 958-63.

13.	Ma, J., Yang, Q., Wen, Y., and Liu, W., *Fe-g-C3N4/graphitized mesoporous carbon composite as an effective Fenton-like catalyst in a wide pH range.* Applied Catalysis B: Environmental, 2017. **201**: p. 232-240.

14.	Lima, M.J., Silva, C.G., Silva, A.M.T., Lopes, J.C.B., Dias, M.M., and Faria, J.L., *Homogeneous and heterogeneous photo-Fenton degradation of antibiotics using an innovative static mixer photoreactor.* Chemical Engineering Journal, 2017. **310**: p. 342-351.

15.	Ong, W.J., Tan, L.L., Ng, Y.H., Yong, S.T., and Chai, S.P., *Graphitic Carbon Nitride (g-C3N4)-Based Photocatalysts for Artificial Photosynthesis and Environmental Remediation: Are We a Step Closer To Achieving Sustainability?* Chem Rev, 2016. **116**(12): p. 7159-329.

16.   Orfao, J.J., Silva, A.I., Pereira, J.C., Barata, S.A., Fonseca, I.M., Faria, P.C., and Pereira, M.F., *Adsorption of a reactive dye on chemically modified activated carbons--influence of pH.* J Colloid Interface Sci, 2006. **296**(2): p. 480-9.

17.   Ma, T.Y., Tang, Y., Dai, S., and Qiao, S.Z., *Proton-functionalized two-dimensional graphitic carbon nitride nanosheet: an excellent metal-/label-free biosensing platform.* Small, 2014. **10**(12): p. 2382-9.

18.   Marques, R.R.N., Sampaio, M.J., Carrapiço, P.M., Silva, C.G., Morales-Torres, S., Dražić, G., Faria, J.L., and Silva, A.M.T., *Photocatalytic degradation of caffeine: Developing solutions for emerging pollutants.* Catalysis Today, 2013. **209**: p. 108-115.

19.   Zhao, H., Chen, S., Quan, X., Yu, H., and Zhao, H., *Integration of microfiltration and visible-light-driven photocatalysis on g-C3N4 nanosheet/reduced graphene oxide membrane for enhanced water treatment.* Applied Catalysis B: Environmental, 2016. **194**: p. 134-140.

20.   Figueiredo, J.L., *Functionalization of porous carbons for catalytic applications.* Journal of Materials Chemistry A, 2013. **1**(33): p. 9351.

21.   Zhu, B., Xia, P., Ho, W., and Yu, J., *Isoelectric point and adsorption activity of porous g-C3N4.* Applied Surface Science, 2015. **344**: p. 188-195.

APPENDIX A

Initially was made a calibration line for H_2O_2 measurement, Figure 1, Abs = 0.22 [H_2O_2] + 0.022 and R^2 = 0.9975. For that were prepared different samples using H_2O UP and know H_2O_2 concentrations, Figure 2.
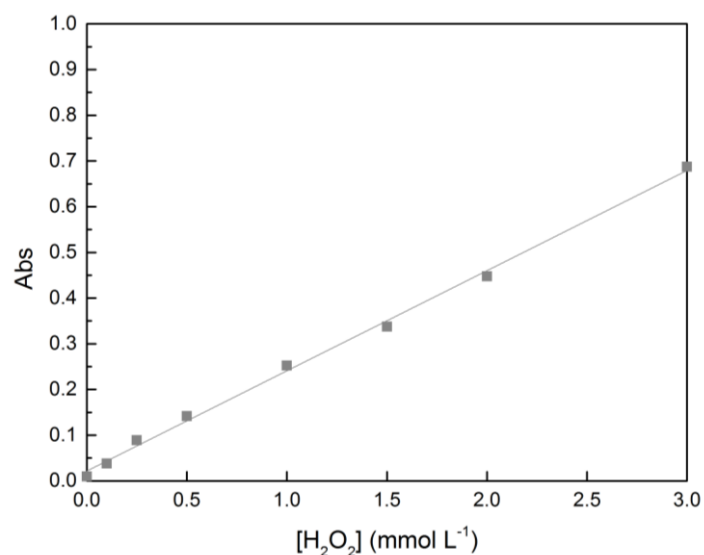
Figure 1 – Calibration line for H_2O_2 measurement.

Figure 2 – Solutions prepared for the calibration line for H_2O_2 measurement.

In Table 1 are the volumes of H_2O_2 added for each volumetric flask and also the H_2SO_4 and Titaniom (IV) oxysulfate volumes. The 0.5 M H_2SO_4 solution was prepared adding 5.61 mL of H_2SO_4 in a 200 mL volumetric flask and ultrapure water. In the next figure are the different samples used in this experimental setup.

Table 1 – Volumes of H_2O_2 added for each volumetric flask and also the H_2SO_4 and Titaniom (IV) oxysulfate volumes.

Concentration (M)	Volume of H_2O_2 (µL)	Volume of H_2SO_4 (mL)	Volume of Titaniom (IV) oxysulfate (mL)
3	7.67	11.9	1.19
2	5.11	11.9	1.19
1.5	3.83	11.9	1.19
1	2.56	11.9	1.19
0.5	1.28	23.8	2.38
0.25	0.64	47.6	4.76
0.1	0.26	95.2	9.52

In Figure 3 it is represented the abs of those samples for different wave length, in this study the wave length used for read the concentration was 405 nm.
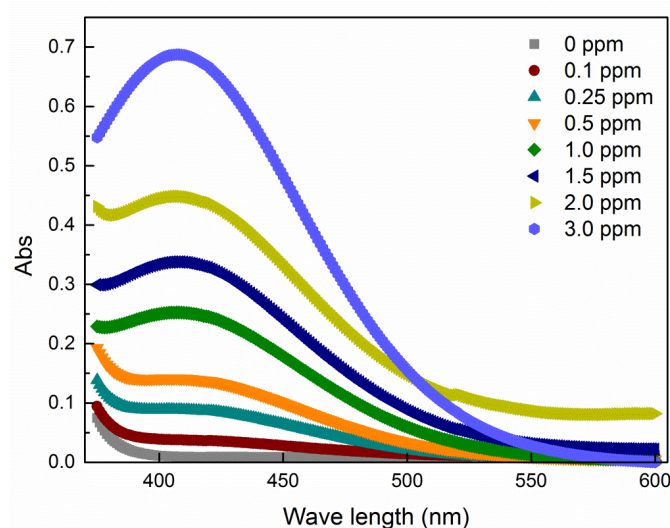
Figure 3 – Spectrum of all samples used in this experimental setup.

Aqueous solutions of target compounds, phenol, were prepared at desired initial concentration then the powered photocatysts are dispersed in the solution with ultrasonication and then mixed with a magnetic stirrer. When it was needed the pH was adjusted with HCl and NaOH solutions. For the preparation of phenol solutions it was used ultrapure water and then the correspondent mass of phenol was weight. HPLC was used for measure the area of the phenol peaks. The calibration line is in the Figure 4, Area = 202895 [PhOH] – 196706, R^2 = 0.9916.
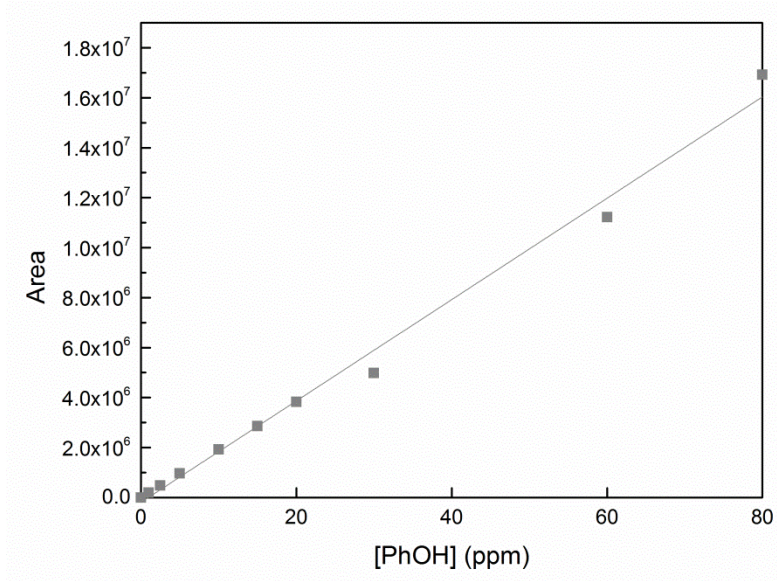
Figure 4 – Calibration line for phenol measurement.